Microwave-based arbitrary CPHASE gates for transmon qubits

George S. Barron [1,*] F. A. Calderon-Vargas,[1] Junling Long,[2] David P. Pappas,[2] and Sophia E. Economou[1,†]

[1]*Department of Physics, Virginia Tech, Blacksburg, Virginia 24061, USA*
[2]*National Institute of Standards and Technology, Boulder, Colorado 80305–3328, USA*

Superconducting transmon qubits are of great interest for quantum computing and quantum simulation. A key component of quantum chemistry simulation algorithms is breaking up the evolution into small steps, which naturally leads to the need for nonmaximally entangling, arbitrary CPHASE gates. Here we design such microwave-based gates using an analytically solvable approach leading to smooth, simple pulses. We use the local invariants of the evolution operator in SU(4) to develop a method of constructing pulse protocols, which allows for the continuous tuning of the phase. We find CPHASE fidelities of more than 0.999 and gate times as low as 100 ns.

I. INTRODUCTION

Quantum computing promises solutions to a number of problems in computing, chemistry, and material science. Superconducting qubits are a promising candidate for qubits because their fabrication relies on existing techniques [1,2], and they can also have their characteristics tailored for specific applications.

Superconducting qubits have been recently used in the implementation of quantum algorithms for molecular problems [3–5], reinforcing the idea that quantum chemistry is one of the most appealing applications of quantum computing [6]. In many quantum simulation algorithms, gate decompositions of Trotterized Hamiltonians often include CPHASE gates, which are then written in terms of two maximally entangling CNOT gates [7]. This decomposition is shown in Fig. 1. Clearly, using CPHASE gates instead of CNOTs would reduce circuit depth and potentially improve resource use in terms of time and fidelity.

Fast high-fidelity two-qubit gates remain challenging in superconducting qubits [8]. Spectral crowding makes accurately addressing an individual transition to produce a controlled operation difficult over short times because the bandwidth required to resolve differences between nearby transitions becomes very small, increasing the time required for each gate [9]. The trade-off is then that either gate times are long or the gate fidelity is low.

One approach to implementing two-qubit gates in superconducting qubits is to dynamically tune elements of the circuit. For example, one can tune the qubit frequency [2,10–14], resonator frequency [15,16], or the coupling strength [17,18]. Unfortunately, tunable elements introduce charge noise, leading to decoherence and low fidelity. An alternative method is to apply microwave pulses to the qubits to drive

transitions that implement unitary rotations [19–33]. Typically, microwave-based control selects a single transition to implement a two-qubit gate. However, spectral crowding is a generic issue for systems controlled exclusively by microwave pulses since, without tuning, their spectra are fixed (to Stark shift effects) and this usually forces the gate time to be very long to spectrally select the target transition. Moreover, the always-on coupling in these systems makes single-qubit gates nontrivial, especially for strongly coupled qubits.

In this work, we develop a collection of microwave-based CPHASE gates using the speeding up wave forms by inducing phases to harmful transitions (SWIPHT) [22] protocol, which overcomes spectral crowding. This protocol was recently used in experiment to produce CNOT gates between two transmon qubits [33]. Here we make use of hyperbolic secant (sech) pulse envelopes [34] which are smooth and simple to implement and produce high fidelities with low gate times for a variety of angles [35,36]. These type of pulses were recently used on transmons in experimental demonstrations of Z gates [37] and as part of a two-qubit gate [28]. We use the local invariants [38,39] of the two-qubit analytic evolution operator with control sech pulses to find conditions on the pulse parameters that achieve the desired two-qubit operation. Through simulations of transmons with typical parameters, we show that our CPHASE gates produce high fidelities for low gate times. These CPHASE gates are applicable in either an all-microwave context or a microwave-tuning hybrid context. Regarding the latter, our CPHASE gates are applicable in the sense that they only rely on a weak effective $Z \otimes Z$ coupling compared to methods that dynamically tune circuit elements. This reliance on only a weak amount of dynamical tuning of the circuit parameters allows these gates to be performed in a variety of parameter regimes. To address the generic challenge of implementing single-qubit gates with fixed-frequency, always-coupled transmons, we design a composite pulse protocol that gives high-fidelity X rotations, which along with our two-qubit gates and previously available Z gates [37,40] form a universal set. These single-qubit gates all take less than 50 ns each and have fidelities in excess of 0.992.

*gbarron@vt.edu
†economou@vt.edu
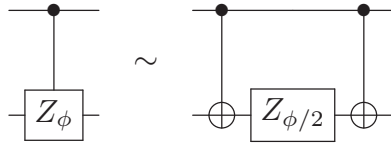
FIG. 1. Nonmaximally entangling CPHASE gate decomposed into two maximally entangling CNOT gates.

This paper is organized as follows. In Sec. II we introduce the two-qubit Hamiltonian for the system of transmons coupled by a resonator. In Sec. III we present the results of the analytical CPHASE protocols and numerical performance, as well as their robustness in other coupling strength regimes. In Sec. IV we present our single-qubit gates along with their fidelities. We conclude in Sec. V.

II. TRANSMON HAMILTONIAN

We focus on two superconducting transmon qubits coupled by a cavity [41]. The transmons are modeled as weakly anharmonic oscillators and the cavity as a harmonic oscillator. The Hamiltonian for this system is given by

$$H_0 = \omega_c a^\dagger a + \sum_{j=1,2} \epsilon_{j,1} a_j^\dagger a_j - \frac{\eta_j}{2} a_j^\dagger a_j (a_j^\dagger a_j - 1)$$
$$+ g_j (a_j^\dagger a + a^\dagger a_j), \qquad (1)$$

where ω_c is the frequency of the cavity connecting the two qubits, $\epsilon_{j,1}$ is the transition frequency between the ground and first excited states for the jth qubit, η_j is the anharmonicity of the jth qubit, g_j is the coupling strength between the cavity and the jth qubit, a ($a^\dagger$) is the annihilation (creation) operator for the cavity, and a_j ($a_j^\dagger$) is the annihilation (creation) operator for the jth qubit. The Hamiltonian describing the coupling to the external microwave electric field is given by

$$H_p(t) = \sum_{j=1,2} E_j(t) e^{i\omega_{p,j} t} a_j + \text{H.c.}, \qquad (2)$$

where $E_j(t)$ and $\omega_{p,j}$ are the pulse envelope and frequency driving the jth qubit, respectively. For the design of our gates we only drive (without loss of generality) the second qubit so that $E_1(t) = 0$, $E_2(t) = E(t)$, and $\omega_{p,2} = \omega_p$.

The states in the system are $|i; j, k\rangle = |i\rangle_c |j, k\rangle$, where $|i\rangle_c$ is the ith cavity level and the jth (kth) index denotes the level of the first (second) transmon. It is advantageous to write out the Hamiltonian in the dressed basis [42], which diagonalizes H_0, and the indices of each element of the dressed basis is determined by the state in the bare basis that has the largest overlap with the dressed state. For example, for indices s_i we write an element of the dressed basis as an eigenstate of H_0 with $|\widetilde{s_1}\rangle = \sum_i \alpha_i |s_i\rangle$, where $|\alpha_1| > |\alpha_i|$ with $i \neq 1$. We encode each qubit into the lowest two levels of each transmon. Consequently, the projection operator for the two-qubit subspace is $P_{\text{QSS}} = |\widetilde{0; 0, 0}\rangle \langle \widetilde{0; 0, 0}| + |\widetilde{0; 0, 1}\rangle \langle \widetilde{0; 0, 1}| + |\widetilde{0; 1, 0}\rangle \langle \widetilde{0; 1, 0}| + |\widetilde{0; 1, 1}\rangle \langle \widetilde{0; 1, 1}|$. Going to the dressed basis and projecting into the qubit subspace spanned by the basis $|\widetilde{0; 0, 0}\rangle, |\widetilde{0; 0, 1}\rangle, |\widetilde{0; 1, 0}\rangle, |\widetilde{0; 1, 1}\rangle$, the approximate two-qubit Hamiltonian when only one qubit is

driven is given by

$$H_{\text{QSS}} \approx \begin{bmatrix} -\omega_{I,1}/2 & \Omega_1(t)e^{i\omega_p t} & 0 & 0 \\ \Omega_1(t)^* e^{-i\omega_p t} & +\omega_{I,1}/2 & 0 & 0 \\ 0 & 0 & -\omega_{I,2}/2 & \Omega_2(t)e^{i\omega_p t} \\ 0 & 0 & \Omega_2(t)^* e^{-i\omega_p t} & +\omega_{I,2}/2 \end{bmatrix}. \qquad (3)$$

The block-diagonal approximation here corresponds to neglecting the presence of the cross-resonance interaction that is introduced when strongly driving qubits at or near the frequency of neighboring qubits. Our pulses are limited to comparatively small driving fields so we expect the cross-resonance effect to be negligible. Indeed, this is confirmed by our numerical simulations. We define $\delta\omega_I$ as the difference between the transition frequencies of the two subspaces $\omega_{I,1}$ and $\omega_{I,2}$ each corresponding with subspace 1 (upper left block) and subspace 2 (lower right block) of the Hamiltonian, respectively, as well as $\Omega_i(t) = E(t)d_i$ for the dipole moment d_i of each transition. Here we have made the approximation that terms in the Hamiltonian that couple states with a different number of excitations on the first qubit will vanish. This is due to the fact that in the dressed basis, since our off-diagonal coupling terms in H_0 are small compared to the diagonal terms, $|\langle \widetilde{i; j, k}|i; j, k|$ is large compared to contributions from other states.

To design fast gates, we avoid spectrally selecting one of the two subspaces and allow the pulse to drive both transitions. Because in general $d_1 \neq d_2$ and $\omega_{I,1} \neq \omega_{I,2}$, the same $E(t)$ on each block will produce different evolutions. Our goal is to design control pulses $E(t)$ that generate two-qubit gates of the form $|0\rangle \langle 0| \otimes \mathbb{I}_2 + |1\rangle \langle 1| \otimes U$, and other control pulses that generate single-qubit gates of the form $\mathbb{I}_2 \otimes U$.

III. CPHASE GATES

For each of the following CPHASE gates, we use hyperbolic secant pulses of the form $\Omega(t) = \Omega_0 \text{sech}(\sigma t)$ with bandwidth σ, amplitude Ω_0, and pulse frequency ω_p. This pulse is chosen because it gives an analytically solvable time-dependent Schrödinger equation for a two-level system [34], is smooth, and has nice analytic properties for rotations about the Z axis [35] (see Appendix A for the derivation of the evolution operator and discussion of its properties). Specifically, for detuning Δ and bandwidth σ, a 2π hyperbolic secant pulse will induce a phase $2\arctan(\sigma/\Delta)$ and a 4π pulse will induce a phase $2\arctan\left[\frac{4\Delta/\sigma}{(\Delta/\sigma)^2 - 3}\right]$ [36]. A plot of two examples of hyperbolic secant pulses is shown in Fig. 2. The main idea is that the same sech pulse acts on both (target and harmful) transitions, causing a cyclic evolution to each subspace. This assumes that the dipoles of the two transitions are the same, which is not strictly the case. Nevertheless, approximately equal dipoles, as is the case for the parameters here, suffice for high fidelities. Due to the different detunings of the two transitions from the pulse, each acquires a different phase. The choice of phases for the two transitions, which we can control through the bandwidth and frequency of the pulse, determines the specific CPHASE gate. Since we focus on CPHASE gates, we use 2π and 4π pulses, which only implement cyclic transitions between energy levels. Our pulses generate generalized CPHASE gates,
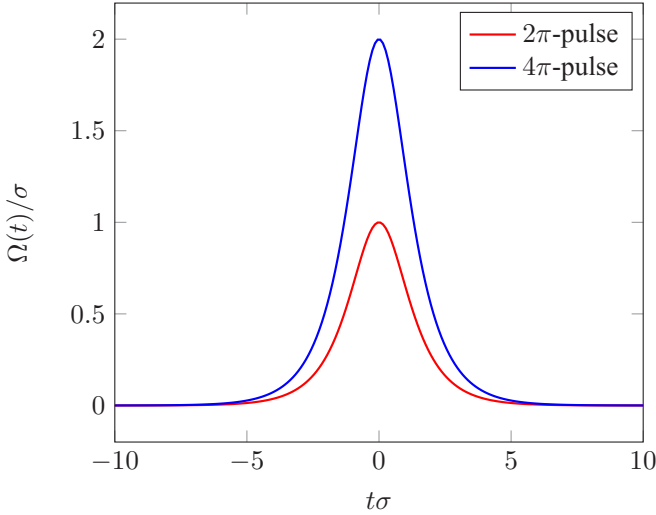
FIG. 2. Hyperbolic secant 2π (lower curve) and 4π (upper curve) pulses. These two different pulse areas have different algebraic properties, which lead to different types of protocols.

FIG. 3. Transitions between two-qubit states. The purple transitions (labeled $\omega_{I,1}$ and $\omega_{I,2}$) correspond to the IQSS protocols, and the orange transitions (labeled $\omega_{O,1}$ and $\omega_{O,2}$) correspond to the OQSS protocols.

defined as $\text{CPHASE}' = \text{diag}(e^{i\phi_{00}}, e^{i\phi_{01}}, e^{i\phi_{10}}, e^{i\phi_{11}})$, which is equivalent to a regular CPHASE gate, $\text{CPHASE} = (1, 1, 1, e^{i\theta})$, up to local Z rotations. The phases in both the generalized and regular CPHASE gates satisfy $\theta = \phi_{00} - \phi_{01} - \phi_{10} + \phi_{11}$. In systems of transmons, it has been shown that zero-duration single-qubit Z rotations may be accomplished by shifting the phase of the microwave pulse [40], so this generalization does not affect our gate times or fidelities. Moreover, as discussed in Appendix A, the pulse areas considered here produce no transfer of population and hence only perform rotations about the Z axis. For this reason, although the local invariants allow us to consider arbitrary evolutions in SU(4) up to arbitrary rotations in SU(2) (see Appendix B), our pulses only require that we consider local operations of the form $R_Z(\phi)$, which, as discussed above, do not affect gate times or fidelities.

In the following results, we denote protocols that use transitions that exist inside the qubit subspace as "IQSS" and protocols that use transitions partially outside the qubit subspace as "OQSS." These two sets of transitions are illustrated in Fig. 3. In particular, when we refer to a protocol that is "IQSS," the transitions and their respective frequencies that we consider are $\omega_{I,1} : |\widetilde{0;00}\rangle \leftrightarrow |\widetilde{0;01}\rangle$, $\omega_{I,2} : |\widetilde{0;10}\rangle \leftrightarrow |\widetilde{0;11}\rangle$. On the other hand, if the protocol is "OQSS," then the transitions and their respective frequencies that we consider are $\omega_{O,1} : |\widetilde{0;01}\rangle \leftrightarrow |\widetilde{0;02}\rangle$, $\omega_{O,2} : |\widetilde{0;11}\rangle \leftrightarrow |\widetilde{0;12}\rangle$. As per the SWIPHT protocol, in either of these cases we designate either the IQSS or OQSS transitions with either the harmful or target transitions with transition frequencies $\omega_{x,h}$ and $\omega_{x,t}$, respectively. From these we define the difference $\delta\omega_x = \omega_{x,t} - \omega_{x,h}$ with $x \in \{I, O\}$ depending on the transitions chosen.

When evaluating the performance of the derived protocols, we numerically solve the Schrödinger equation to obtain the evolution operator at the end of each pulse. In our simulations we keep 3 states for the cavity and 4 states for each of the qubits, so that the Hilbert space simulated is 48 dimensional. This sufficiently simulates the full dynamics of the system in that adding more available states does not change our
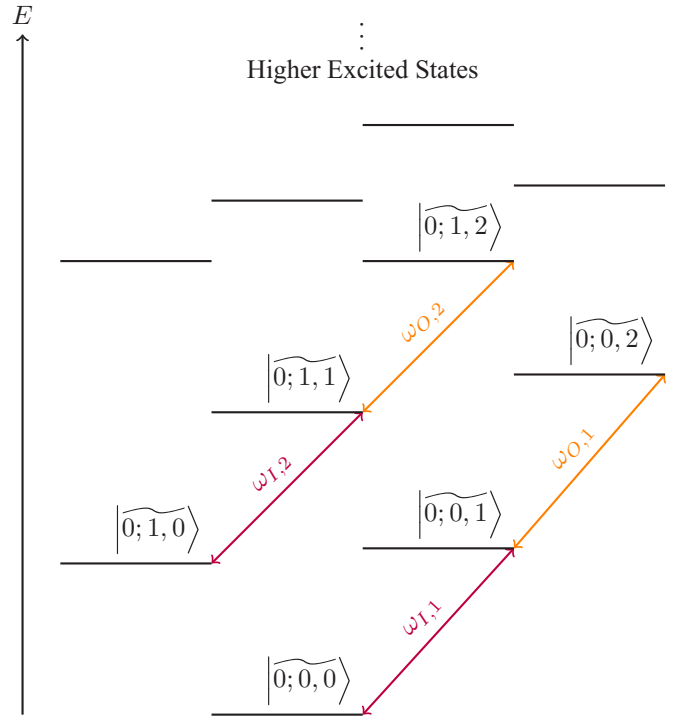
resulting fidelities. To compare the final evolution operator we obtain from the simulation with the target one, we calculate the fidelity given by $F = \frac{1}{n(n+1)}[\text{Tr}(MM^\dagger) + |\text{Tr}(M)|^2]$ [43], where $M = U_0^\dagger U$, with U_0 being the desired gate and U being the actual gate from simulations. Each U and U_0 are truncated so that they act only on the qubit subspace. In our numerical simulations we use $\omega_c = 7.15$ GHz, $\epsilon_{1,1} = 6.2$ GHz, $\epsilon_{2,1} = 6.8$ GHz, $\eta_1 = \eta_2 = \eta = 350$ MHz, and $g_1 = g_2 = g = 130$ MHz as the fixed parameters, except in Sec. III B, where we evaluate the performance of the gates when varying the coupling strength g. From these, we find that $\delta\omega_I = 3.23$ MHz and $\delta\omega_O = -11.07$ MHz. Bell-shaped pulses such as Gaussians or hyperbolic secants used here theoretically extend to infinity. In practice, of course, experimentalists switch on and off the pulses at finite times. Similarly, simulations require truncation of the pulses. We choose the gate time such that the simulation runtime is reasonable without sacrificing accuracy. We find that $T = 10/\sigma$ [which corresponds to $\Omega(T)/\Omega_0 \approx 0.01347$] suffices to achieve this. Moreover, we numerically optimize around the analytically predicted solution to compensate for errors such as a difference in the dipoles of the two transitions. Below we describe each of the protocols and provide results from numerical simulations quantifying their performance.

A. CPHASE gate via off-resonant 2π-pulse OQSS

Our strategy here is to find conditions on the bandwidth and pulse frequency of a hyperbolic secant pulse that performs a generalized CPHASE gate on the two subspaces defined above.

To this end, we use the local invariants (Appendix B) of the analytical evolution operator for the two-qubit system driven by sech pulses (Appendix A).

First, we recall that the definition of the generalized CPHASE gate is $\mathrm{CPHASE}' = \mathrm{diag}(e^{i\phi_{00}}, e^{i\phi_{01}}, e^{i\phi_{10}}, e^{i\phi_{11}})$, where the phase imparted is $\theta = \phi_{00} - \phi_{01} - \phi_{10} + \phi_{11}$. If we consider the two block-diagonal portions of the Hamiltonian H_{QSS} (3), then we can define two detunings between the pulse and the desired transitions, $\Delta_1 = \omega_p - \omega_{O,1}$ and $\Delta_2 = \omega_p - \omega_{O,2}$.

Now for the OQSS protocol the block-diagonal form of the Hamiltonian as well as the analytical solution for the unitary operator of a two-level system discussed in Appendix A allows us to write the evolution operator as $U = \mathrm{diag}(1, f_1, 1, f_2)$. Here $f_j = {}_2F_1(-a, +a, \frac{-i\Delta_j + \sigma}{2\sigma}, 1)$ is the Gaussian hypergeometric function with $a \equiv \frac{\Omega}{\sigma} \in \mathbb{Z}$. Using Eq. (B3) We can compute the local invariants of the two-qubit evolution operator U, yielding

$$G_1(U) = \tfrac{1}{8}(4 + \gamma + \gamma^*),$$
$$G_2(U) = 0,$$
$$G_3(U) = 2 + \frac{\gamma}{2}, \tag{4}$$

where

$$\gamma = \frac{\Gamma^2\left(\frac{\sigma - i\Delta_1}{2\sigma}\right) \Gamma\left(-a + \frac{1}{2} - \frac{i\Delta_2}{2\sigma}\right) \Gamma\left(a + \frac{1}{2} - \frac{i\Delta_2}{2\sigma}\right)}{\Gamma^2\left(\frac{\sigma - i\Delta_2}{2\sigma}\right) \Gamma\left(-a + \frac{1}{2} - \frac{i\Delta_1}{2\sigma}\right) \Gamma\left(a + \frac{1}{2} - \frac{i\Delta_1}{2\sigma}\right)}$$
$$+ \frac{\Gamma^2\left(\frac{\sigma - i\Delta_2}{2\sigma}\right) \Gamma\left(-a + \frac{1}{2} - \frac{i\Delta_1}{2\sigma}\right) \Gamma\left(a + \frac{1}{2} - \frac{i\Delta_1}{2\sigma}\right)}{\Gamma^2\left(\frac{\sigma - i\Delta_1}{2\sigma}\right) \Gamma\left(-a + \frac{1}{2} - \frac{i\Delta_2}{2\sigma}\right) \Gamma\left(a + \frac{1}{2} - \frac{i\Delta_2}{2\sigma}\right)}. \tag{5}$$

We also compute the local invariants for the target CPHASE gate, yielding

$$\mathbf{G}[\mathrm{diag}(1, 1, 1, e^{i\theta})] = [\cos(\theta/2)^2, 0, 2 + \cos(\theta)], \tag{6}$$

where $\mathbf{G}(U) = (G_1(U), G_2(U), G_3(U))$.

In order to find the conditions on the pulse parameters, we demand that the local invariants of U [Eq. (4)] be equal to those of the CPHASE gate, and thus we arrive at (assuming for simplicity that $a = 1$)

$$\cos\theta = \cos[\phi_1(\Delta_1) - \phi_1(\Delta_2)], \tag{7}$$

where $e^{i\phi_1(\Delta_j)} = \frac{\sigma - i\Delta_j}{\sigma + i\Delta_j}$.

For the IQSS protocol, we follow the same procedure, except that in that case the IQSS evolution operator is $U = \mathrm{diag}(f_1, f_1^*, f_2, f_2^*)$ After imposing that the respective local invariants of U and the CPHASE gate be equal, for a 2π pulse we arrive at

$$\cos\theta = \cos\{2[\phi_1(\Delta_1) - \phi_1(\Delta_2)]\}. \tag{8}$$

In our parameter regime, the IQSS protocol has similar or lower performance than the OQSS protocol, and thus in the remainder of this section we focus on the OQSS protocol only.

In the SWIPHT protocol, there is a notion of a "harmful" and "target" transition. The difference between these two transitions is that we select the "harmful" transition to be the transition that we want to drive to obtain a trivial phase. The "target" transition then corresponds to the transition that looks like the target portion of a controlled unitary operation. So here we see that there is some freedom in defining which

of the two blocks (1 or 2) involves the target and which the harmful transition. We define the following choice of sign:

$$\lambda = \begin{cases} +1 & \text{Target is block 1} \\ -1 & \text{Target is block 2} \end{cases}. \tag{9}$$

We also define Δ_t and Δ_h based on this choice. Then noting that $\omega_p = \Delta_h + \omega_h = \Delta_t + \omega_t$ and defining $\delta\omega_O = \omega_t - \omega_h$, we can use the definitions for θ, ϕ_1 as well as trigonometric identities to find $\delta\omega_O/\sigma = \cot[\phi_1(\Delta_h)/2] - \cot[\phi_1(\Delta_t)/2]$.

Now if we specify an angle for the two-qubit gate, then all of the restrictions up until now allow us to find a pulse frequency and bandwidth that perform two different rotations on each block, but together they combine to form a CPHASE operation. We define $\theta_1 = \phi_{00} - \phi_{01}$, $\theta_2 = \phi_{10} - \phi_{11}$ as well as $\theta = \theta_1 + \theta_2$, $\delta\theta = \theta_1 - \theta_2$. These can be written in terms of the harmful/target detunings and λ as follows: $\theta = \lambda[\phi_1(\Delta_t) - \phi_1(\Delta_h)]$ and $\delta\theta = \phi_1(\Delta_t) + \phi_1(\Delta_h)$. With these expressions we can then find an expression for the bandwidth in terms of the desired angle,

$$\sigma = \lambda\delta\omega_O \frac{\cos(\theta/2) - \cos(\delta\theta/2)}{2\sin(\theta/2)}. \tag{10}$$

To successfully generate an arbitrary CPHASE gate we also need to express the control pulse frequency ω_p in terms of the desired θ angle. In this line, using previous definitions for ω_p, we can write $\omega_p = \frac{\omega_t + \omega_h}{2} + \frac{1}{2}(\Delta_t + \Delta_h)$, which can be easily rewritten in terms of θ and $\delta\theta$:

$$\omega_p = \frac{\omega_t + \omega_h}{2} + \frac{1}{2}(\Delta_t + \Delta_h)$$
$$= \frac{\omega_t + \omega_h}{2} + \sigma \frac{\sin(\delta\theta/2)}{\cos(\theta/2) - \cos(\delta\theta/2)}.$$

Using Eq. (10) to further simplify the previous equation, we find that the pulse frequency in terms of the desired angle θ is

$$\omega_p = \frac{\omega_{O,t} + \omega_{O,h}}{2}$$
$$+ \lambda \frac{\delta\omega_O}{2\sin(\theta/2)} \sqrt{1 - [\cos(\theta/2) - 2\sin(\theta/2)\sigma/\delta\omega_O]^2}, \tag{11}$$

where, in order to ensure that the resulting pulse has finite frequency, we require that the angle of the CPHASE gate is within the range $\theta \in (0, \pi]$. Moreover, to make the pulse frequency real, this expression also provides a maximum allowable bandwidth for a given angle θ, $\sigma_{\max} = \frac{|\delta\omega_O|}{2} \cot(\theta/4)$.

Using this protocol, we find fidelities in excess of 0.999 and gate times as low as 60 ns. The numerical evaluations of the fidelity in the simulation for this protocol are shown in Fig. 4. From the figure we see that the fidelity is consistently above 0.992 for all angles and gate times. By choosing smaller bandwidths, one is able to increase the fidelity. The infidelity at small gate times is due to leakage outside the qubit subspace.

B. CPHASE gate via resonant pulses

The construction of the protocols presented in this section is similar to that of the off-resonant protocols in Sec. III A, with the difference that now we require the pulses to be
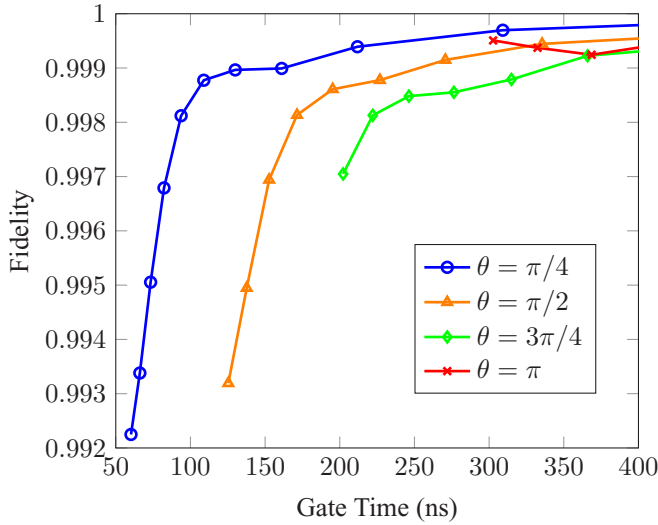
FIG. 4. Fidelity of numerical simulations for the CPHASE gate with the OQSS protocol. For every angle, there is a maximum allowable bandwidth and hence a minimum allowable gate time.

resonant with one of the two transitions in the system. In this family of protocols, we will first restrict the value $a = \Omega/\sigma \in \mathbb{Z}$ so that each subspace sees a rotation about the Z axis, independent of the detuning with the frequency of each transition.

For the IQSS case, this means that the evolution operator is diagonal and has the form $U = \mathrm{diag}(f_1, f_1^*, f_2, f_2^*)$, where $f_j = {_2F_1}(-a, +a, \frac{-i\Delta_j + \sigma}{2\sigma}, 1)$. Because we are constructing resonant protocols, without loss of generality, we let the pulse be resonant with the first transition so that $\Delta_1 = 0$ and $\Delta_2 = \delta\omega_I$. We may then compute the local invariants, yielding

$$\mathbf{G}(U) = \left[\frac{\mathrm{Re}(\alpha)^2}{|\alpha|^2}, 0, 2 + \frac{1}{2}\left(\frac{\alpha}{\alpha^*} + \frac{\alpha^*}{\alpha} \right) \right], \qquad (12)$$

where $\alpha = {_2F_1}(-a, +a, \frac{-i\delta\omega_I + \sigma}{2\sigma}, 1)$ is the Gaussian hypergeometric function. Then, demanding that the local invariants of the CPHASE gate [Eq. (6)] be equal to the evolution operator for the pulsed system yields a single equation for this protocol:

$$\cos\theta = \frac{\alpha^2 + \alpha^{*2}}{2|\alpha|^2}. \qquad (13)$$

As an example, for a 2π pulse we let $a = 1$. Then this equation reduces to

$$\frac{\delta\omega_I^4 - 6\delta\omega_I^2\sigma^2 + \sigma^4}{\left(\delta\omega_I^2 + \sigma^2\right)^2} = \cos\theta. \qquad (14)$$

Solving this equation for the bandwidth yields four solutions, and because the bandwidth must be positive, only two are physical based on the sign of $\delta\omega_I$. For the $a = 1$ case, the final bandwidths are

$$\sigma_1 = |\delta\omega_I| \cot(\theta/4), \qquad (15)$$

$$\sigma_2 = |\delta\omega_I| \tan(\theta/4). \qquad (16)$$

This procedure may be repeated for pulses with $a \in \mathbb{N}$, though the resulting equations are more complicated and

may be treated numerically. Additionally, one may repeat this protocol while using the OQSS transitions. The setup is essentially the same, except the OQSS evolution operator will be

$$U = \mathrm{diag}(1, f_1, 1, f_2). \qquad (17)$$

In this case, the analogous single equation for these protocols will be

$$\cos\theta = (-1)^a \frac{1 + \alpha^2}{2\alpha}, \qquad (18)$$

where now $\alpha = {_2F_1}(-a, +a, \frac{+i\delta\omega_O + \sigma}{2\sigma}, 1)$ For OQSS transitions, where the control sech pulse is resonant with a transition partially out of the qubit space, the derivation of the protocols rely on solving Eq. (18) for the bandwidth of the pulse. In particular, for a sech 2π pulse ($a = 1$) we find that the associated bandwidth that produces a CPHASE gate for a given angle is $\sigma = |\delta\omega_O| \cot(\theta/2)$, where again we require that $\theta \in (0, \pi]$. On the other hand, if we instead use a 4π pulse, then the solution to the evolution operator has different properties compared to the resonant 2π case, and we find that the bandwidth for a specific angle $\theta \in (0, \pi)$ is given by

$$\sigma = |\delta\omega_O| \frac{\tan(\theta/2)}{\sqrt{4 + 3\tan(\theta/2)^2 \pm 2}}. \qquad (19)$$

In this case, the choice of sign is arbitrary and the bandwidth does not depend on which transition is designated as the harmful or target. However, the choice of sign determines the range of the bandwidth. We find that if the sign choice is positive, then $0 < \frac{\sigma}{|\delta\omega_O|} < 1/\sqrt{3}$ and if the choice of sign is negative, then $1/\sqrt{3} < \frac{\sigma}{|\delta\omega_O|}$. In some protocols derived here, there are multiple ranges of allowed bandwidths. These ranges result from the fact that multiple bandwidths satisfy Eq. (18) for a given angle and $\delta\omega$. In our parameter regime, this protocol has comparable or lower performance from the others simulated here, so we do not show numerical results in this case.

If we repeat this procedure but now choosing transitions corresponding to the IQSS case, then the different bandwidths are obtained by solving Eq. (13). For example, in the case of a 2π pulse ($a = 1$), the bandwidth for this CPHASE gate of angle $\theta \in (0, \pi]$ is $\sigma = |\delta\omega_I| \cot(\theta/4)$. Here we find gates with fidelities as high as 0.999999 and gate times as low as 24 ns for angles in the range of $\pi/16$ to $\pi/2$. To construct this protocol, the pulse is driven on resonance with one of the transitions inside the qubit subspace. We evaluate the performance of this protocol in simulation by calculating the gate fidelity, shown in Fig. 5. The two curves correspond to the two different choices of resonant transitions. The upper (blue) curve corresponds to the lower right block being the target, and the bottom (red) curve corresponds to the upper left block being the target. We find that the fidelity using subspace 2 as the target is above 0.9998 for angles from $\pi/8$ to $\pi/2$, and using the other transition as the target produces lower fidelities of $\sim$0.9995. In either case, we find reasonable gate times for this range of angles. The infidelity at smaller angles is due to leakage as a result of larger pulse amplitudes. In contrast with the other numerical results, in this protocol the desired angle of the gate fixes the bandwidth and hence the gate time.
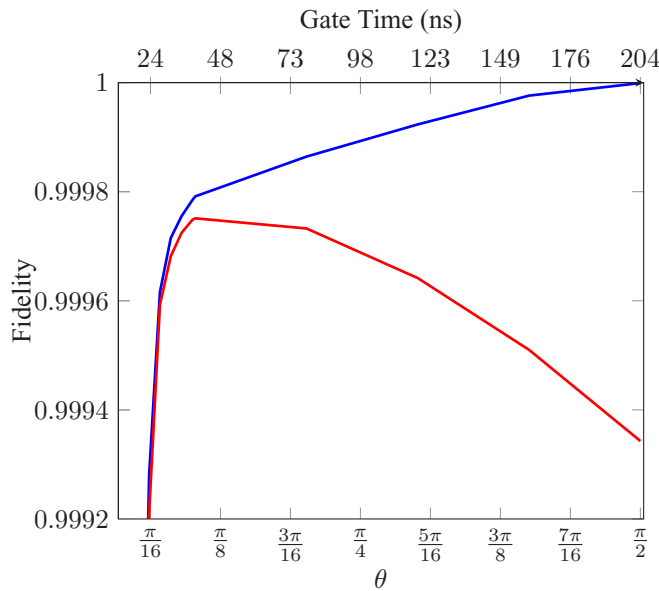
FIG. 5. Performance of CPHASE gate from simulation using the resonant IQSS 2π protocol. The upper curve corresponds to using subspace 2 as the target, $\omega_{I,2} = \omega_t$, and the bottom curve corresponds to using subspace 1 as the target, $\omega_{I,1} = \omega_t$.

When we repeat this procedure for a 4π pulse, the CPHASE gate of angle $\theta \in (0, \pi)$, has bandwidth $\sigma = |\delta\omega_I| \frac{\tan(\theta/4)}{\sqrt{4 + 3\tan(\theta/4)^2} \pm 2}$. Again, the pulse is driven on resonance with one of the transitions inside the qubit subspace. We also find that the range on the bandwidth in the case when the choice of sign is positive becomes $0 < \frac{\sigma}{|\delta\omega_I|} < \frac{1}{2 + \sqrt{7}}$ and when the choice of sign is negative, we have $\frac{1}{\sqrt{7} - 2} < \frac{\sigma}{|\delta\omega_I|}$.

So far we have fixed the coupling to $g = 130$ MHz. Now we focus on the IQSS 2π protocol and evaluate its performance as a function of the coupling strength. We determine two primary features as we vary the coupling strength. First, weakly coupled systems produce gate times that increase rapidly as a function of the desired angle, as shown in Fig. 6. Second, increasing the coupling strength decreases the fidelity, as shown in Fig. 6. Overall, we find that for a range of coupling strengths we are able to find high

fidelities exceeding 0.998. In some cases the fidelity is as high as 0.999999. In all cases, the fidelity drops for smaller angles due to leakage as a result of larger pulse amplitudes. We limit these simulations to 200 ns gate durations to compare the different coupling strengths because this protocol has no upper bound on the gate time.

C. CPHASE protocols comparison

In Table I we provide a summary of the results of the various protocols. Overall, we find that there is flexibility in the way of constructing CPHASE gates. For instance, one does not necessarily need to drive on resonance with one of the transitions. Additionally, one may choose various pulse areas or bandwidths for different implementations. For instance, one may choose to derive protocols with $a = 3, 4, \ldots$. This has the potential to reduce the duration of the gate at the cost of potentially introducing more leakage, which one could possibly address by incorporating Derivative Removal by Adiabatic Gate (DRAG) [44–46] into the pulse design, but this is beyond the scope of this work. In terms of performance, the two best protocols are the OQSS arbitrary frequency via 2π-pulse and IQSS resonant 2π-pulse protocols. Comparing the fidelities and gate times for a range of angles, if a small angle is desired one should choose the IQSS resonant 2π-pulse protocol because at small angles it provides consistently higher fidelities (~ 0.9999 compared to ~ 0.998) at comparable gate times and sometimes fidelities as high as 0.999999. On the other hand, if a larger angle is desired, then the OQSS arbitrary frequency via 2π-pulse protocol is preferable due to its flexibility in the bandwidth, yielding potentially lower gate times (~ 120 ns compared to ~ 200 ns). The other protocols produce fidelities on the order of ~ 0.98 generally due to their higher bandwidths, which result in more leakage. In systems that do not have higher available states, these protocols may be more useful as they can produce smaller gate times for a range of angles.

IV. SINGLE QUBIT GATES

Now we turn our attention to single qubit operations. Developing single qubit operations in an always-coupled two-qubit system is inherently challenging. This is because the interaction between the two qubits dresses the energy eigen-

TABLE I. Summary of results for various CPHASE protocols. These results are derived in Secs. III A and III B. Each row denotes the analytical results of a particular protocol producing a CPHASE gate by an angle θ. The way to read this column is from left to right. First, choose a pair of transitions corresponding to the transitions in Fig. 3 and then choose a pulse area. The properties of the selected pulse will then be the bandwidth for a particular angle and the range on such bandwidths. In some cases, there are two disconnected ranges of allowable bandwidths. The OQSS 2π protocol has an arbitrary bandwidth in the sense that it is not a function of the desired angle. However, the bandwidth must satisfy the constraint in the corresponding "Bandwidth range" column.

Transitions	Pulse area	Frequency	Bandwidth	Bandwidth range
IQSS	2π	ω_t	$\sigma = |\delta\omega_I| \cot(\theta/4)$	$0 < \sigma < +\infty$
IQSS	4π	ω_t	$\sigma_\pm = |\delta\omega_I| \frac{\tan(\theta/4)}{\sqrt{4 + 3\tan(\theta/4)^2} \pm 2}$	$0 < \frac{\sigma_+}{|\delta\omega_I|} < \frac{1}{2 + \sqrt{7}} < \frac{1}{-2 + \sqrt{7}} < \frac{\sigma_-}{|\delta\omega_I|} < +\infty$
OQSS	2π	ω_t	$\sigma = |\delta\omega_O| \cot(\theta/2)$	$0 < \sigma < +\infty$
OQSS	4π	ω_t	$\sigma_\pm = |\delta\omega_O| \frac{\tan(\theta/2)}{\sqrt{4 + 3\tan(\theta/2)^2} \pm 2}$	$0 < \frac{\sigma_+}{|\delta\omega_O|} < \frac{1}{\sqrt{3}} < \frac{\sigma_-}{|\delta\omega_O|} < +\infty$
OQSS	2π	Eq. (11)	Arbitrary	$0 < \sigma < \frac{|\delta\omega_O|}{2} \cot(\theta/4) < +\infty$

FIG. 6. Properties and performance of the CPHASE gates using the IQSS 2π protocol over a range of coupling strengths. The upper panel shows the gate time for each coupling strength g as a function of the angle of the CPHASE gate. The middle panel shows the fidelity at each angle for the various coupling strengths using subspace 1 as the target, $\omega_{I,1} = \omega_t$. The lower panel shows the fidelity at each angle for the various coupling strengths using subspace 2 as the target, $\omega_{I,2} = \omega_t$. For all panels, gate times between 10 ns and 200 ns are considered.

states, such that the frequency of the qubit transition in one qubit depends on the state of the other qubit. As a result,

the problem is to find a pulse which implements the same operation in two distinct two-level systems. In the following subsections, we design single-qubit gates by providing two solutions to this problem. One is based on individual Gaussian pulses (Sec. IV A) and the other on sequences of square pulses (Sec. IV B).

A. Gaussian pulse protocol

Here we will design $R_{\hat{z}}(\theta)$ and $R_{\hat{x}}(\pi/2)$ rotations, which can be combined with rotations about Z to give arbitrary single-qubit gates. Since rotations about the Z axis may be produced by shifts in the frequency of the microwave pulse [40] with zero gate time and no loss in fidelity, we only consider the development of the rotations about the x axis.

For this protocol, we use a single Gaussian pulse, $\Omega(t) = \Omega_0 e^{-(\sigma t)^2}$, that is resonant with the transition frequency of the target qubit. Since the qubits are strongly coupled, the $|0\rangle \leftrightarrow |1\rangle$ transition frequency is conditional on the state of the other qubit. Here we choose the frequency when the qubit not being driven is in the $|0\rangle$ state. This pulse has two free parameters, the amplitude Ω_0 and the bandwidth σ. Treating this problem numerically, we will optimize the final fidelity of the evolution operator with the desired evolution operator, $\mathbb{I} \otimes R_{\hat{x}}(\pi/2)$. Accordingly, the evolution operator of the whole system (i.e., including higher levels of the transmons and cavity) is projected into the qubit subspace before calculating the fidelity. We use a Bayesian optimization algorithm, which is useful in cases where calls to the objective function are costly and gradients are not easily be evaluated. This technique has been used in quantum control before [47]. The result of this procedure is a Gaussian pulse with $\Omega_0 = 60.25$ MHz and $\sigma = 67.57$ MHz. Plots of the relevant transition probabilities and the pulse envelope are shown in Figs. 7(a) and 7(b), respectively. The pulse duration is 11.75 ns and the gate has a final fidelity of $F = 0.99563$. Interleaving two copies of this pulse with five rotations about the z axis allows us to perform any single qubit rotation.

B. Square pulse protocol

We also develop $R_{\hat{x}}(\theta)$ rotations via a sequence of square pulses. In this case, the Hamiltonian is simply the Hamiltonian in Eq. (3) for piecewise constant $\Omega_i(t)$ and $\omega_{p,i}(t)$. The evolution operator for the qubit subspace can be written as

$$U(\vec{\tau}, \vec{E}, \vec{\omega}) = \begin{bmatrix} U_1(\vec{\tau}, \vec{E}, \vec{\omega}) & 0 \\ 0 & U_2(\vec{\tau}, \vec{E}, \vec{\omega}) \end{bmatrix}, \quad (20)$$

where $U_j(\vec{\tau}, \vec{E}, \vec{\omega}) = \prod_{i=1}^{N} U_{j,i}(\tau_i, E_i, \omega_{p,i})$ and $U_{j,i}(\tau_i, E_i, \omega_{p,i})$ is the evolution operator for the jth block over the duration of the ith square pulse. The ith square pulse has duration τ_i, pulse amplitude E_i and frequency $\omega_{p,i}$.

Instead of solving exactly for parameters of each pulse that perform the desired evolution on each subspace, we define an objective function to optimize which is $f_{\hat{n},\theta}(\vec{\tau}, \vec{E}, \vec{\omega}) = F(\mathbb{I} \otimes R_{\hat{n}}(\theta), U(\vec{\tau}, \vec{E}, \vec{\omega}))$, where $F(U, V)$ is the fidelity between two unitary operators. We do this for several reasons. Primarily, there is no guarantee that such solutions exist, and even if they did, they would likely not be simple. Moreover, even if we solve for a sequence of pulses

(a)

(b)
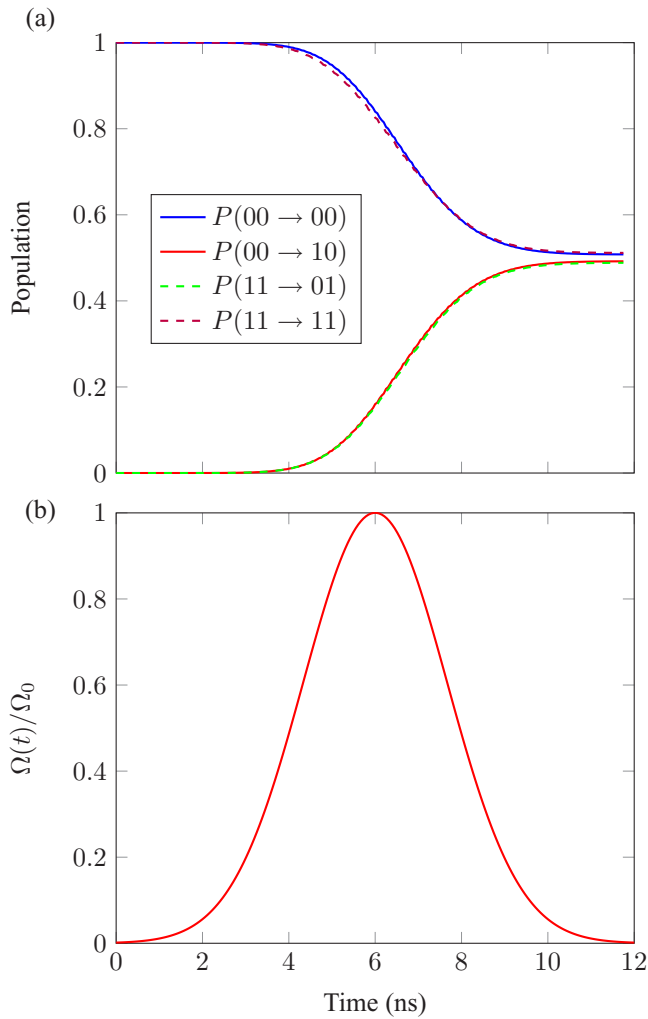
FIG. 7. (a) Plot of the probabilities as a function of time for various transfers of population to and from elements of the computational basis. Since we are performing the rotation $\mathbb{I} \otimes R_{\hat{x}}(\pi/2)$, we expect that the final probabilities shown end up at 1/2. The dashed/solid lines are simply so that the plots do not overlap. (b) Plot of the pulse envelope $\Omega(t)$ as a function of time.

that exactly implements the desired evolution, in simulation and experiment the fidelity will not be exactly 1 due to decoherence. Here we use global, constrained optimization algorithms over the $3N$ parameters to find such sequences of pulses. The region in which the optimization is performed is determined by experimental limitations such as ramp-up times for the microwave pulses on the order of 1 ns and maximum possible amplitudes of each pulse based on the microwave pulse generators of about 20 MHz.

The desired evolution operator for the qubit subspace here is $\mathbb{I} \otimes R_{\hat{x}}(\theta)$ so that $U_j(\vec{\tau}, \vec{E}, \vec{\omega}) = R_{\hat{x}}(\theta)$ for each $j = 1, 2$. Without loss of generality, we choose a sequence of pulses resonant with the first subspace so that $\omega_{p,i} = \omega_{I,1}$. Then, with $E_i \in \mathbb{R}$, this sequence of square pulses naturally produces rotations about the x axis for the first subspace, $R_{\hat{x}}(\theta) = U_1(\vec{\tau}, \vec{E}, \vec{\omega})$. This provides the constraint $\theta/2 = d_1 \sum_{i=1}^{N} \tau_i |E_i|$. Now the optimization is over $2N$ parameters with one constraint.
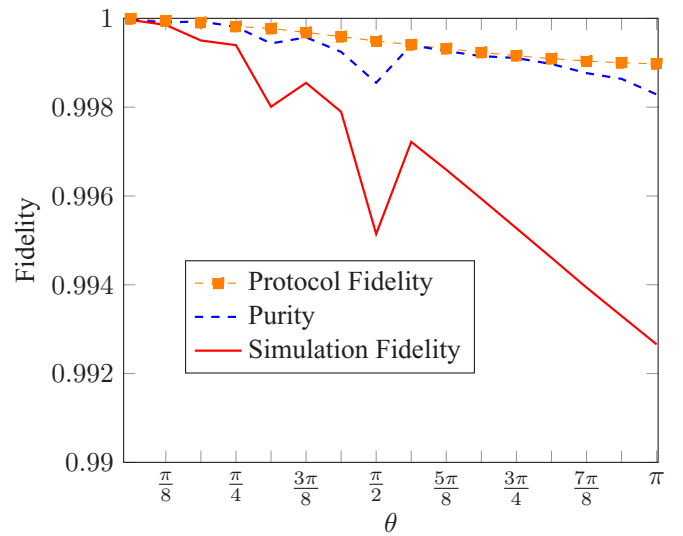
FIG. 8. Performance of single qubit rotation protocol. The upper (orange) curve is the protocol fidelity, determined by global optimization over the parameters of a sequence of resonant square pulses for the four-level system. The middle (blue) curve is the purity as a function of the angle. The bottom (red) curve is the fidelity found from simulation of the full time dynamics of the system after using the result from the protocol as an initial condition in a local optimization.

We evaluate the performance of the single qubit X rotation protocol. This involves two steps: The first step is to determine the parameters on some sequence of square pulses by the optimization of $f_{\hat{n},\theta}(\vec{\tau}, \vec{E}, \vec{\omega})$, which yields what we define as the "protocol fidelity," see Fig. 8. The second step is to take the resulting sequence of square pulses and simulate the full time dynamics of the system, using a local optimization to improve the results of the protocol in the simulation. This is done by using the parameters of each pulse sequence from the protocol as initial conditions to a local optimization algorithm that improves the fidelity. We refer to this as the "simulation fidelity" in Fig. 8. We find "simulation fidelities" above 0.992 for all angles $0 < \theta \leqslant \pi$. All of these gates have durations from $\sim$15 ns to $\sim$25 ns. Because there is a gap between the "simulation fidelity" and purity in the figure, we see that there is some coherent error occurring. This is due to coupling to higher excited states which are not included in the four-level system and is the primary cause of the infidelity. The dip at $\theta = \pi/2$ is due to the fact that we use a local optimizer for the "simulation Ffidelity" and the curve is not guaranteed to be smooth.

V. CONCLUSIONS

Using the analytical evolution operator for the hyperbolic secant pulse acting on a two-level system, we have derived a collection of CPHASE gates for transmon qubits. We have demonstrated that these gates produce high fidelities typically in excess of $\sim$0.999 and in some cases as high as 0.999999 and typical gate times less than $\sim$100 ns. Moreover, we show that one of these protocols is robust in the fidelity for a range of angles and coupling strengths g. Finally, we

demonstrate that arbitrary single qubit gates may be achieved via microwave control in this parameter regime using either single Gaussian pulses or sequences of square pulses. Our high-fidelity parameterized entangling gates may be applied in realistic systems for use in quantum simulation algorithms.

APPENDIX A: HYPERBOLIC SECANT PULSE SOLUTION

The basis for the CPHASE gate is the analytic solution for the evolution operator of a two-level system driven by a hyperbolic secant pulse. The pulse is defined as $\Omega(t) = \Omega_0 \text{sech}(\sigma t)$, where σ is the pulse bandwidth and Ω_0 is the pulse strength. One can show that the form of the Hamiltonian for a given transition in the interaction frame is

$$H_2(t) = \begin{bmatrix} 0 & \Omega(t)e^{i\Delta t} \\ \Omega(t)^* e^{-i\Delta t} & 0 \end{bmatrix}, \qquad \text{(A1)}$$

where Δ is the detuning of the pulse with the $|0\rangle \leftrightarrow |1\rangle$ transition, i.e., $\Delta = \omega_p - \epsilon_1$. By following a previous discussion of this problem [35], we define $c = \frac{1}{2}(1 + i\frac{\Delta}{\sigma})$, $a = \frac{\Omega}{\sigma}$, $\zeta = \frac{1}{2}[1 + \tanh(\sigma t)]$, $\alpha(a, c, \zeta) = {}_2F_1(a, -a, c^*, \zeta)$, and $\beta(a, c, \zeta) = {}_2F_1(a + 1 - c, 1 - a - c, 2 - c, \zeta)$ where ${}_2F_1$ is one of Gauss's hypergeometric functions. Then the evolution operator is

$$U(t, -\infty) = \begin{bmatrix} \alpha(a, c, \zeta) & -\frac{ia}{c}\zeta^c \beta(a, c, \zeta) \\ -\frac{ia}{c^*}\zeta^{c^*} \beta(a, c, \zeta)^* & \alpha(a, c, \zeta)^* \end{bmatrix}. \qquad \text{(A2)}$$

Here the initial condition is $U(-\infty, -\infty) = \mathbb{I}$, though in practice we take the initial time to be some finite value that is sufficiently large for our results to converge. Since we are only interested in the end result of the pulse, we consider the evolution operator at $t = +\infty$,

$$U = U(+\infty, -\infty)$$
$$= \begin{bmatrix} {}_2F_1\left(-a, a; \frac{\sigma - i\Delta}{2\sigma}; 1\right) & -i\text{sech}\left(\frac{\pi\Delta}{2\sigma}\right)\sin(a\pi) \\ -i\text{sech}\left(\frac{\pi\Delta}{2\sigma}\right)\sin(a\pi) & {}_2F_1\left(-a, a; \frac{i\Delta + \sigma}{2\sigma}; 1\right) \end{bmatrix}. \qquad \text{(A3)}$$

Then it is clear that for $a \in \mathbb{Z}$, the evolution operator is diagonal. In this instance, we can express the evolution operator with $U = \text{diag}\{e^{-i\phi_a}, e^{+i\phi_a}\}$. If we use a 2π pulse (i.e., $a = 1$), then $\phi_1(\Delta) = 2\arctan\left(\frac{\sigma}{\Delta}\right)$. If instead we consider a 4π pulse, then $a = 2$ and $\phi_2(\Delta) = 2\arctan\left[\frac{4\Delta/\sigma}{(\Delta/\sigma)^2 - 3}\right]$.

APPENDIX B: LOCAL INVARIANTS

To develop our CPHASE gates, we will use the local invariants [38,39] of unitary operations in SU(4), denoted here as G_i for $i \in \{1, 2, 3\}$. These are three quantities that may be computed from any element of SU(4) and are invariant under operations in SU(2). That is, for $\mathcal{U} \in \text{SU}(4)$ and $V_i \in \text{SU}(2)$,

$$G_i(V_1 \otimes V_2 \, \mathcal{U} \, V_3 \otimes V_4) = G_i(\mathcal{U}). \qquad \text{(B1)}$$

Therefore, the local invariants convey the nonlocal properties of the operator $\mathcal{U}$ and give a unique representation of any class of two-qubit gates that are equivalent up to local operations. Note that single-qubit rotations about the Z axis may be efficiently performed for transmons [40] and that hyperbolic secant pulses can produce no population transfer, as discussed in Appendix A and in Ref. [36]. These two facts allow us to develop protocols for CPHASE operations that only consider their nonlocal characteristics and have no overhead in terms of the fidelity or time required to perform the single-qubit gates associated with their local-equivalence classes. Hence, the local invariants of the analytical unitary evolution, U, for our four-level system driven by a hyperbolic secant pulse will be the starting place for constructing our protocols for a CPHASE gate. The quantities G_i are obtained by first placing U in the magic basis [48] defined by the unitary transformation [38,39]

$$Q = \frac{1}{\sqrt{2}} \begin{pmatrix} 1 & 0 & 0 & i \\ 0 & i & 1 & 0 \\ 0 & i & -1 & 0 \\ 1 & 0 & 0 & -i \end{pmatrix}. \qquad \text{(B2)}$$

The local invariants are the coefficients of the characteristic polynomial of the matrix $M(U) = (Q^\dagger U Q)^T (Q^\dagger U Q)$, and they are given by the following expressions:

$$G_1 = \text{Re}\frac{\text{tr}[M(U)]^2}{16 \det U},$$
$$G_2 = \text{Im}\frac{\text{tr}[M(U)]^2}{16 \det U},$$
$$G_3 = \frac{\text{tr}[M(U)]^2 - \text{tr}[M^2(U)]}{4 \det U}. \qquad \text{(B3)}$$

[1] L. Frunzio, A. Wallraff, D. Schuster, J. Majer, and R. Schoelkopf, Fabrication and characterization of superconducting circuit QED devices for quantum computation, IEEE Trans. Appl. Supercond. **15**, 860 (2005).

[2] J. Majer, J. M. Chow, J. M. Gambetta, J. Koch, B. R. Johnson, J. A. Schreier, L. Frunzio, D. I. Schuster, A. A. Houck, A. Wallraff, A. Blais, M. H. Devoret, S. M. Girvin, and R. J. Schoelkopf, Coupling superconducting qubits via a cavity bus, Nature **449**, 443 (2007).

[3] A. Kandala, A. Mezzacapo, K. Temme, M. Takita, M. Brink, J. M. Chow, and J. M. Gambetta, Hardware-efficient variational quantum eigensolver for small molecules and quantum magnets, Nature **549**, 242 (2017).

[4] J. I. Colless, V. V. Ramasesh, D. Dahlen, M. S. Blok, M. E. Kimchi-Schwartz, J. R. McClean, J. Carter, W. A. de Jong, and I. Siddiqi, Computation of Molecular Spectra on a Quantum Processor with an Error-Resilient Algorithm, Phys. Rev. X **8**, 011021 (2018).

[5] P. J. J. O'Malley, R. Babbush, I. D. Kivlichan, J. Romero, J. R. McClean, R. Barends, J. Kelly, P. Roushan, A. Tranter, N. Ding, B. Campbell, Y. Chen, Z. Chen, B. Chiaro, A. Dunsworth, A. G. Fowler, E. Jeffrey, E. Lucero, A. Megrant, J. Y. Mutus, M. Neeley, C. Neill, C. Quintana, D. Sank, A. Vainsencher, J. Wenner, T. C. White, P. V. Coveney, P. J. Love, H. Neven, A. Aspuru-Guzik, and J. M. Martinis, Scalable Quantum Simulation of Molecular Energies, Phys. Rev. X **6**, 031007 (2016).

[6] J. Preskill, Quantum Computing in the NISQ era and beyond, Quantum **2**, 79 (2018).

[7] I. M. Georgescu, S. Ashhab, and F. Nori, Quantum simulation, Rev. Mod. Phys. **86**, 153 (2014).

[8] X. Gu, A. F. Kockum, A. Miranowicz, Y.-x. Liu, and F. Nori, Microwave photonics with superconducting quantum circuits, Phys. Rep. **718-719**, 1 (2017).

[9] L. S. Theis, F. Motzoi, and F. K. Wilhelm, Simultaneous gates in frequency-crowded multilevel systems using fast, robust, analytic control shapes, Phys. Rev. A **93**, 012324 (2016).

[10] L. DiCarlo, J. M. Chow, J. M. Gambetta, L. S. Bishop, B. R. Johnson, D. I. Schuster, J. Majer, A. Blais, L. Frunzio, S. M. Girvin, and R. J. Schoelkopf, Demonstration of two-qubit algorithms with a superconducting quantum processor, Nature **460**, 240 (2009).

[11] L. DiCarlo, M. D. Reed, L. Sun, B. R. Johnson, J. M. Chow, J. M. Gambetta, L. Frunzio, S. M. Girvin, M. H. Devoret, and R. J. Schoelkopf, Preparation and measurement of three-qubit entanglement in a superconducting circuit, Nature **467**, 574 (2010).

[12] J. Ghosh, A. Galiautdinov, Z. Zhou, A. N. Korotkov, J. M. Martinis, and M. R. Geller, High-fidelity controlled-σ^z gate for resonator-based superconducting quantum computers, Phys. Rev. A **87**, 022309 (2013).

[13] J. M. Martinis and M. R. Geller, Fast adiabatic qubit gates using only σ_z control, Phys. Rev. A **90**, 022307 (2014).

[14] R. Barends, J. Kelly, A. Megrant, A. Veitia, D. Sank, E. Jeffrey, T. C. White, J. Mutus, A. G. Fowler, B. Campbell, Y. Chen, Z. Chen, B. Chiaro, A. Dunsworth, C. Neill, P. O'Malley, P. Roushan, A. Vainsencher, J. Wenner, A. N. Korotkov, A. N. Cleland, and J. M. Martinis, Superconducting quantum circuits at the surface code threshold for fault tolerance, Nature **508**, 500 (2014).

[15] D. C. McKay, S. Filipp, A. Mezzacapo, E. Magesan, J. M. Chow, and J. M. Gambetta, Universal Gate for Fixed-Frequency Qubits Via a Tunable Bus, Phys. Rev. Appl. **6**, 064007 (2016).

[16] M. Roth, M. Ganzhorn, N. Moll, S. Filipp, G. Salis, and S. Schmidt, Analysis of a parametrically driven exchange-type gate and a two-photon excitation gate between superconducting qubits, Phys. Rev. A **96**, 062323 (2017).

[17] Y. Chen, C. Neill, P. Roushan, N. Leung, M. Fang, R. Barends, J. Kelly, B. Campbell, Z. Chen, B. Chiaro, A. Dunsworth, E. Jeffrey, A. Megrant, J. Y. Mutus, P. J. J. O'Malley, C. M. Quintana, D. Sank, A. Vainsencher, J. Wenner, T. C. White, M. R. Geller, A. N. Cleland, and J. M. Martinis, Qubit

Architecture with High Coherence and Fast Tunable Coupling, Phys. Rev. Lett. **113**, 220502 (2014).

[18] B. Royer, A. L. Grimsmo, N. Didier, and A. Blais, Fast and high-fidelity entangling gate through parametrically modulated longitudinal coupling, Quantum **1**, 11 (2017).

[19] A. Galiautdinov, Generation of high-fidelity controlled-NOT logic gates by coupled superconducting qubits, Phys. Rev. A **75**, 052303 (2007).

[20] J. M. Chow, A. D. Córcoles, J. M. Gambetta, C. Rigetti, B. R. Johnson, J. A. Smolin, J. R. Rozen, G. A. Keefe, M. B. Rothwell, M. B. Ketchen, and M. Steffen, Simple All-Microwave Entangling Gate for Fixed-Frequency Superconducting Qubits, Phys. Rev. Lett. **107**, 080502 (2011).

[21] J. M. Chow, J. M. Gambetta, A. W. Cross, S. T. Merkel, C. Rigetti, and M. Steffen, Microwave-activated conditional-phase gate for superconducting qubits, New J. Phys. **15**, 115012 (2013).

[22] S. E. Economou and E. Barnes, Analytical approach to swift nonleaky entangling gates in superconducting qubits, Phys. Rev. B **91**, 161405(R) (2015).

[23] S. Sheldon, E. Magesan, J. M. Chow, and J. M. Gambetta, Procedure for systematically tuning up cross-talk in the cross-resonance gate, Phys. Rev. A **93**, 060302(R) (2016).

[24] H. Paik, A. Mezzacapo, M. Sandberg, D. T. McClure, B. Abdo, A. D. Córcoles, O. Dial, D. F. Bogorin, B. L. T. Plourde, M. Steffen, A. W. Cross, J. M. Gambetta, and J. M. Chow, Experimental Demonstration of a Resonator-Induced Phase Gate in a Multiqubit Circuit-Qed System, Phys. Rev. Lett. **117**, 250502 (2016).

[25] X.-H. Deng, E. Barnes, and S. E. Economou, Robustness of error-suppressing entangling gates in cavity-coupled transmon qubits, Phys. Rev. B **96**, 035441 (2017).

[26] J. L. Allen, R. Kosut, J. Joo, P. Leek, and E. Ginossar, Optimal control of two qubits via a single cavity drive in circuit quantum electrodynamics, Phys. Rev. A **95**, 042325 (2017).

[27] E. Barnes, C. Arenz, A. Pitchford, and S. E. Economou, Fast microwave-driven three-qubit gates for cavity-coupled superconducting qubits, Phys. Rev. B **96**, 024504 (2017).

[28] T. Noh, G. Park, S.-G. Lee, W. Song, and Y. Chong, Construction of controlled-NOT gate based on microwave-activated phase (MAP) gate in two transmon system, Sci. Rep. **8**, 13598 (2018).

[29] E. Magesan and J. M. Gambetta, Effective Hamiltonian models of the cross-resonance gate, arXiv:1804.04073.

[30] D. J. Egger, M. Ganzhorn, G. Salis, A. Fuhrer, P. Müller, P. K. Barkoutsos, N. Moll, I. Tavernelli, and S. Filipp, Entanglement Generation in Superconducting Qubits using Holonomic Operations, Phys. Rev. Appl. **11**, 014017 (2019).

[31] V. Tripathi, M. Khezri, and A. N. Korotkov, Operation and intrinsic error budget of two-qubit cross-resonance gate, Phys. Rev. A **100**, 012301 (2019).

[32] J. L. Allen, R. Kosut, and E. Ginossar, Minimal time robust two qubit gates in circuit QED, arXiv:1902.08056.

[33] S. P. Premaratne, J.-H. Yeh, F. C. Wellstood, and B. S. Palmer, Implementation of a generalized controlled-NOT gate between fixed-frequency transmons, Phys. Rev. A **99**, 012317 (2019).

[34] N. Rosen and C. Zener, Double Stern-Gerlach experiment and related collision phenomena, Phys. Rev. **40**, 502 (1932).

[35] S. E. Economou, L. J. Sham, Y. Wu, and D. G. Steel, Proposal for optical u(1) rotations of electron spin trapped in a quantum dot, Phys. Rev. B **74**, 205415 (2006).

[36] S. E. Economou, High-fidelity quantum gates via analytically solvable pulses, Phys. Rev. B **85**, 241401(R) (2012).

[37] H. S. Ku, J. L. Long, X. Wu, M. Bal, R. E. Lake, E. Barnes, S. E. Economou, and D. P. Pappas, Single qubit operations using microwave hyperbolic secant pulses, Phys. Rev. A **96**, 042339 (2017).

[38] Y. Makhlin, Nonlocal properties of two-qubit gates and mixed states, and the optimization of quantum computations, Quant. Info. Proc. **1**, 243 (2002).

[39] J. Zhang, J. Vala, S. Sastry, and K. B. Whaley, Geometric theory of nonlocal two-qubit operations, Phys. Rev. A **67**, 042313 (2003).

[40] D. C. McKay, C. J. Wood, S. Sheldon, J. M. Chow, and J. M. Gambetta, Efficient Z gates for quantum computing, Phys. Rev. A **96**, 022330 (2017).

[41] J. Koch, T. M. Yu, J. Gambetta, A. A. Houck, D. I. Schuster, J. Majer, A. Blais, M. H. Devoret, S. M. Girvin, and R. J. Schoelkopf, Charge-insensitive qubit design derived from the Cooper pair box, Phys. Rev. A **76**, 042319 (2007).

[42] C. Cohen-Tannoudji, J. Dupont-Roc, and G. Grynberg, *Atom-Photon Interactions: Basic Processes and Applications* (J. Wiley, New York, 1992).

[43] L. H. Pedersen, N. M. Møller, and K. Mølmer, Fidelity of quantum operations, Phys. Lett. A **367**, 47 (2007).

[44] F. Motzoi, J. M. Gambetta, P. Rebentrost, and F. K. Wilhelm, Simple Pulses for Elimination of Leakage in Weakly Nonlinear Qubits, Phys. Rev. Lett. **103**, 110501 (2009).

[45] J. M. Gambetta, F. Motzoi, S. T. Merkel, and F. K. Wilhelm, Analytic control methods for high-fidelity unitary operations in a weakly nonlinear oscillator, Phys. Rev. A **83**, 012308 (2011).

[46] F. Motzoi and F. K. Wilhelm, Improving frequency selection of driven pulses using derivative-based transition suppression, Phys. Rev. A **88**, 062318 (2013).

[47] F. Sauvage and F. Mintert, Optimal quantum control with poor statistics, arXiv:1909.01229.

[48] C. H. Bennett, D. P. DiVincenzo, J. A. Smolin, and W. K. Wootters, Mixed-state entanglement and quantum error correction. Phys. Rev. A **54**, 3824 (1996).